Available online at www.sciencedirect.com
SCIENCE DIRECT®
Polymer 45 (2004) 993–1005
polymer
www.elsevier.com/locate/polymer

Development of the skin layer in injection moulding: phenomenological model

J.C. Viana*

Department of Polymer Engineering, University of Minho, Campus Azurem, 4800-058 Guimarães, Portugal

Received 19 August 2003; accepted 2 December 2003

Abstract

This work explores the conditions affecting the development of the skin layer in injection moulding. The thermomechanical environment is varied by systematic changes on the operative processing parameters for three moulding geometries: an axi-symmetric tensile bar, a lateral gated disc and a two-point central gated box. The thermomechanical environments are evaluated by computer simulations, by the local bulk temperature and shear stress level. The calculation of dimensionless numbers (Cameron, Brinkman and Nahme) allows the interpretation of the main physical phenomena occurring in the distinct moulding geometries. The relationships between the imposed thermomechanical environment and the thickness of the skin layer are established. For all the mouldings the skin thickness decreases with the increase in the thermal and shear stress levels, although with distinct contributions for the different moulding geometries. The development of the skin layer is interpreted in the light of a phenomenological model involving two time variables: the time allowed for relaxation of the highly oriented melt until the crystallization temperature is reached and the relaxation time of the material. The influence of the operative processing parameters on both time variables are discussed and used to interpret the experimental variations of the thickness of skin layer.
© 2003 Published by Elsevier Ltd.

Keywords: Skin thickness; Thermomechanical environment; Thickening mechanisms

1. Introduction

Injection moulding is a well established processing method to produce plastic parts for engineering applications. In this process the polymer melt is subject to a complex thermomechanical environment characterized by high cooling rates and important stress fields. This environment varies along the flow path and through the thickness of the moulding. As a consequence, a moulded polymer shows an intrinsic heterogeneous microstructure, featuring a gradual and hierarchical variation of the morphology that evolves throughout the spatial domain of the part. For a semi-crystalline polymer a typical layered arrangement is developed, normally referred to as the skin-core microstructure, which can be observed by polarized light microscopy (PLM). The number of identified layers depends on the resolution of the experimental technique used and on the level of discrimination considered. A simple analysis assumes a three-layer model (two external skins and an interior core) [1–5], but other layers may be discerned (e.g. two outer skins, two sub-skin regions, two intermediate shear zones and an inner core). The intrinsic molecular nature of the polymer together with the magnitude of these layers and their morphological state determine the mechanical behaviour of the injection moulded engineering components.

The thermomechanical environment imposed to the polymer during processing is governed by several factors, which include:

(i) the adjustment of the operative processing parameters (machine settings);
(ii) the part geometry and mould design (e.g. part thickness, feeding system, gating options, cooling system);
(iii) the material properties (thermal, rheological and physical properties).

Consequently all these factors will also control the development of the microstructure of the mouldings. The effect of the operative processing variables on the

* Tel.: +351-253-510-335; fax: +351-253-510-339.
E-mail address: jcv@dep.uminho.pt (J.C. Viana).

0032-3861/$ - see front matter © 2003 Published by Elsevier Ltd.
doi:10.1016/j.polymer.2003.12.001

morphological state of the mouldings has been widely study in the last decades [1–18,22–29]. The influence of the material characteristics (e.g. molecular weight, fillers) has also been addressed [3,10–12]. However, the direct link between the operative variables and material features and the morphological parameters is not a satisfactory route. In fact, the proper approach is to relate the local thermomechanical environment to the morphology developed, that is, these relationships should be established locally [13–16]. This approach requires the evaluation of the local thermomechanical environment, which can be quantitatively described by computer simulations of the injection moulding process [13–16] or by adequate mould instrumentation.

The mechanical behaviour of injection moulded parts is determined to some extent by the microstructure developed upon processing. Several morphological features have been identified to dictate these types of relationships. The thickness of the skin layer has been evidenced as a highly significant microstructural parameter [5,10,13–18]. The understanding of the skin formation and the development of predictive tools enabling the estimation of the skin thickness are therefore of crucial importance.

This work explores the conditions affecting the development of the skin layer in injection moulding. The thermomechanical environment is varied by systematic changes on the operative processing parameters for three moulding geometries and estimated by computer simulations of mould filling process. The relationships between the imposed thermomechanical environment and the skin layer thickness are established and interpreted in the light of a phenomenological model intended to interpret its formation.

2. Thermomechanical environment and microstructure development

2.1. Thermomechanical environment

The relative importance of the principal physical phenomena occurring in the injection moulding process and their degree of interaction can be quantified by the calculation of dimensionless numbers [19,20]. The principal ones are defined in Table 1.

The Cameron number, Ca, relates the heat conduction in the thickness direction to the heat convection in the longitudinal one. If $Ca \gg 1$ then the heat conduction dominates, while for $Ca \ll 10^{-2}$ it becomes negligible and the flow can be assumed as occurring in 'quasi-adiabatic' conditions (heat convection in the longitudinal direction dominates). In the interval $10^{-2} < Ca < 1$ the temperature profile is in development and the flow is in a transition regime. The Brinkman number, Br, is the ratio between the heat generated by viscous dissipation and the heat exchanged by conduction through the moulding boundaries. $Br \gg 1$ indicates a strong effect of the heat generated by viscous dissipation on the through-the-thickness temperature profile, whereas for $Br \ll 1$ it can be neglected. The Nahme number, Na, relates the viscous heat generation to the heat required to significantly alter the melt viscosity, η. For $Na \ll 1$, the increase in temperature due to viscous dissipation is not sufficient to change the melt viscosity, which varies mainly with the imposed shear rate and temperature difference at the boundaries. The dimensionless numbers analysis has been used to interpret the main physical phenomena occurring in injection moulding of different part geometries and processing conditions, allowing a better comparison between them [13,15,20].

Table 1
Principal dimensionless numbers

Number	Definition
Cameron, Ca	$Ca = \frac{\alpha X_{cond}}{V X_{conv}^2}$
Brinkman, Br	$Br = \frac{\eta V^2}{K(T_b - T_w)}$
Nahme, Na	$Na = \frac{\eta V^2}{K}(\partial\eta/\partial T)$

(α—thermal diffusivity; $X_{cond/conv}$—characteristic dimension to conduction/convection; V—characteristic velocity; η—viscosity; K—thermal conductivity; $(T_b - T_w)$—imposed temperature difference at the boundaries; T_b—melt average (bulk) temperature; T_w—mould temperature; $\zeta = (\partial\eta/\partial T)$—viscosity thermal dependence coefficient).

In the injection moulding process the thermal and mechanical phenomena are strongly coupled [14,15]. The thermomechanical environment to which the polymer is subjected during the moulding cycle can be estimated by numerical simulations of the process. These simulations allow the local computation of the thermomechanical variables (e.g. temperatures, pressures, shear rates and stresses). The through-the-thickness temperature profile shows a minimum value at the mould wall (where the temperatures variations are steeper: higher cooling rates) and maximum values at the centre (where the cooling rates are much more slow). The local thermal level may be estimated by the bulk temperature, T_b, defined as a velocity weighted average temperature through the moulding thickness [15,21,22]. The shear stress shows a linear profile through the thickness, being zero at the flow centreline and reaching a maximum at the solid/melt interface. This latter value, τ_w, can then be used to evaluate the shear stress level applied to the polymer melt. Both these thermomechanical variables have been used to define the so-called thermomechanical indices, which aimed at interpreting the microstructure development in injection moulding [13–16,22,23].

2.2. Skin development

During the injection phase of the moulding cycle, the forward motion of the screw, at a given velocity, pushes the polymer melt into a mould with the desired part shape. When the hot polymer-melt contacts the cold mould walls, it

automatically freezes off (high thermal choc), creating a solid frozen layer. This phenomenon imparts important consequences:

(i) the reduction of the flow cross-sectional area increasing the pressure drop to fill the cavity;
(ii) the creation of an insulation barrier due to the low thermal conductivity of the polymer, leading to a slower cooling rate of the inner material.

For a given material, the frozen layer thickness depends basically on the local thermal conditions, which may vary during the filling phase. The amount of solidified material evolutes dynamically as result of the temperature changes due to viscous dissipation.

The complex combination of the imposed stress field and huge cooling rate strongly affects the crystallization kinetics and the resultant crystalline morphology of the skin layer. Its morphology has been studied by several authors [13,14,24,25], featuring a highly oriented shish-kebab like structure. When observed by PLM the skin has a homogeneous appearance with no discernable morphological features [26].

The thickness of the skin layer is controlled by the combined effect of the thermal and the stress field imposed during processing [13,14,27], both determining the cooling and crystallization conditions. It has been proposed that the skin thickness is determined by the material relaxation time and by the rate of cooling [28]. The development of the skin layer has also been interpreted in the light of two main factors: the time allowed for relaxation until the crystallization temperature is reached and the material relaxation time [14]. The skin formation is thermally controlled for high melt temperatures and governed by the stress level for lower temperatures [14,22,27]. The skin-core boundary is located between a non-flow isothermal and the maximum shear rate locus [27]. A thicker skin is obtained for lower (melt and mould) temperatures and flow rates [3–10,14]. The skin thickness decreases with the reduction of the molecular weight of the material [3,10,27], and by narrowing its distribution [29]. The use of nucleating agents affecting the crystallization conditions has also a strong effect on the thickness (and orientation level) of the skin layer [12].

3. Experimental and numerical

3.1. Material and moulding

The material used in this work is a propylene copolymer (APPRYL 3120 MR5). The moulding programme considered three different geometries as shown in Fig. 1: (i) a tensile axi-symmetric specimen with 1.5 mm diameter; (ii) a lateral gated disc (1.5 mm thick); and (iii) a two gate-points box with a thickness of 1.5 mm.

The injection moulding conditions also considered systematic variations in the melt and mould temperatures (T_{inj} and T_w, respectively) and the injection flow rate, Q_{inj}, according to Table 2.

3.2. Microstructure observation

From all mouldings, 15 μm thick samples were cut transversely to the flow direction using a LEISTRZ microtome in pre-determined locations (see Fig. 1):

(i) at the middle of the circular cross-section of the tensile specimens;
(ii) at the centre of the circular disc;
(iii) at 26.5 mm from both edges of the box moulding.

For the box mouldings, additional cuts were also obtained in the flow direction (at the same position). The microtomed samples were observed by PLM, evidencing the typical skin-core microstructures. The skin thickness was measured in ten points and averaged. The measurements were performed in a calibrated image analyzer system (Quantimed 500C) coupled to the microscope. The average experimental scatter was less than 6.6, 3.0 and 4.5%, respectively, for the axi-symmetric tensile, the disc and the box mouldings. The skin ratio, Sa, was defined as the quotient between the thickness of the skin and of the overall moulding cross-section.

3.3. Mould filling simulations

The thermomechanical environment imposed to the melt during processing was characterized by computer simulations of the mould filling stage (C-MOLD software). Only the filling phase was considered. The material was assumed as a shear thinning fluid with temperature dependence ($\eta = 19,200\dot{\gamma}^{-0.645}e^{-0.00783T}$, T in °C). The thermomechanical variables envisaged were the bulk temperature, T_b, and the shear stress at the melt/solid interface, τ_w. They were locally computed at the same position where the microtomed cross-sections for microscopy observations were obtained.

4. Results

4.1. Dimensionless numbers

The main physical phenomena occurring during the injection moulding stages (filling and cooling) were evaluated by the dimensionless numbers (Table 1). Their calculation aimed only at comparing the main physical phenomena occurring in the distinct moulding geometries [15].

Fig. 2 presents the variations of Ca with the flow rate (the variations of Q_{inj} were normalized relatively to the selected

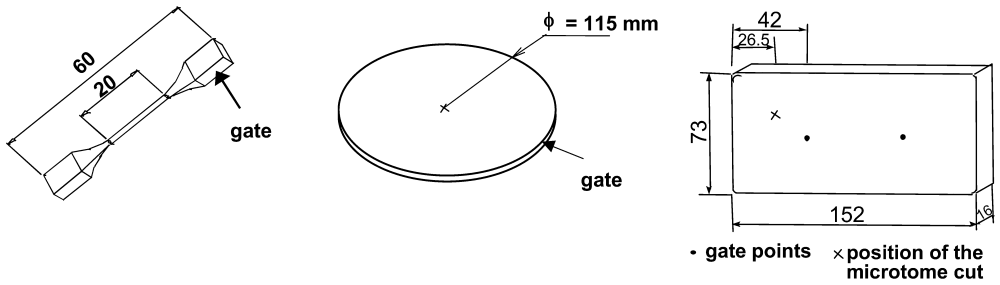

Fig. 1. Geometry of the moulding (all with 1.5 mm of thickness).

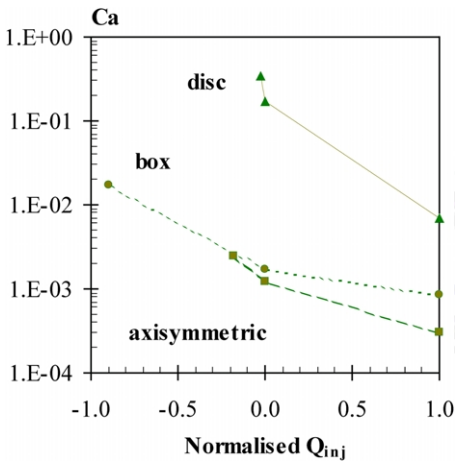

Fig. 2. Variation of the Cameron number, Ca, with the processing variables for the three geometries.

maximum (1.0) and minimum (−1) values). The disc mouldings show the highest Ca numbers as a result of the highest heat losses by conduction through the mould walls. The tensile axi-symmetric specimens present the lowest Ca values. The box mouldings show similar Ca values except that the variations upon Q_{inj} are higher (see also Table 2). For these mouldings the flow can be generally considered as 'quasi-adiabatic' since $Ca < 10^{-2}$, meaning that the heat convection in the flow direction prevails over the heat conduction through the thickness.

Fig. 3 shows the variations of Br with the processing variables (their variations were normalized relatively to the selected maximum (1.0) and minimum (−1) values). The axi-symmetric specimen presents the highest heat generated by viscous dissipation (highest Br), which significantly alters the melt viscosity (moulding also showing the highest Na, as depicted in Fig. 4). These effects are much lower in the plate-like mouldings, the disc showing the lowest values of Br and Na. For these two mouldings, and in a higher level for the disc mouldings, the heating due to the viscous dissipation is very small compared with the heat exchanged by conduction through the mould walls. The melt viscosity is mainly controlled by the shear rate and the temperature differences imposed at the boundaries.

Table 2
Moulding conditions for the three geometries

Moulding geometry									
Run	Tensile axi-symmetric specimen			Laterally gated disc			Box moulding		
	T_{inj} (°C)	T_w (°C)	Q_{inj} (cm^3/s)	T_{inj} (°C)	T_w (°C)	Q_{inj} (cm^3/s)	T_{inj} (°C)	T_w (°C)	Q_{inj} (cm^3/s)
1	200	5	40	190	5	92	220	20	200
2	200	5	5	190	5	2	250	20	100
3	200	30	10	190	30	4	280	20	10
4	200	80	40	190	80	92	220	50	100
5	200	80	5	190	80	2	250	50	10
6	230	5	10	230	5	4	280	50	200
7	230	30	40	230	30	92	220	80	10
8	230	30	10	230	30	4	250	80	200
9	230	30	5	230	30	2	280	80	100
10	230	80	10	230	80	4	–	–	–
11	270	5	40	280	5	92	–	–	–
12	270	5	5	280	5	2	–	–	–
13	270	30	10	280	30	4	–	–	–
14	270	80	40	280	80	92	–	–	–
15	270	80	5	280	80	2	–	–	–
Max	270	80	40	280	80	92	280	80	200
Min	200	5	5	190	5	2	220	20	10
Δ(Max − Min)	70	75	35	90	75	90	60	60	190

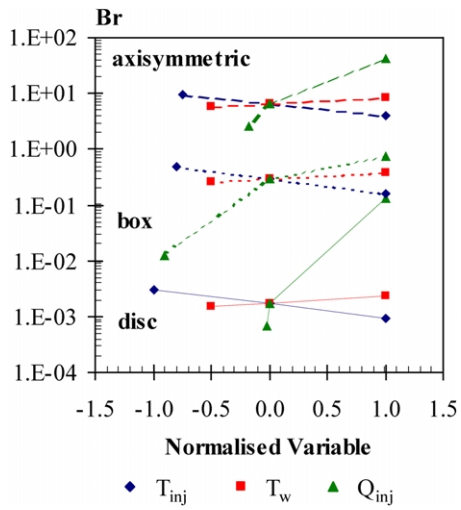

Fig. 3. Variation of the Brinkman, Br, number with the processing variables for the three moulding geometries.

4.2. Thermomechanical variables

Table 3 lists the values of the thermomechanical variables for the three moulding geometries. The maximum values of T_b are similar for all the moulding geometries. The disc mouldings show the higher T_b variations (lowest T_b values), already anticipated by the highest values of Ca numbers. This moulding also presents the lowest τ_w values, despite having the highest range of variation. The highest τ_w are found for the tensile specimens, which evidenced the highest Br numbers.

Fig. 5 presents the variations of the computed bulk temperature and maximum shear stress with the processing variables for the tensile specimen geometry. These dependences are plotted relatively to the flow rate and the imposed temperature differences ($T_{inj} - T_w$). T_b increases with both Q_{inj} and the imposed temperature difference, as expected. This corresponds to a higher thermal level and

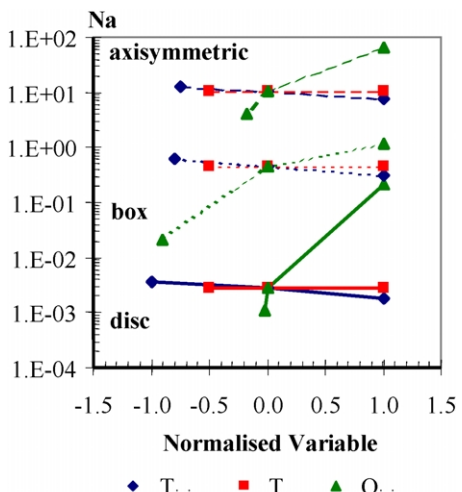

Fig. 4. Variation of the Nahme, Na, number with the processing variables for the three moulding geometries.

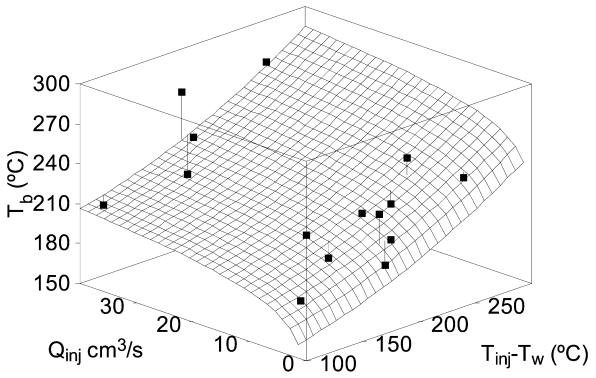

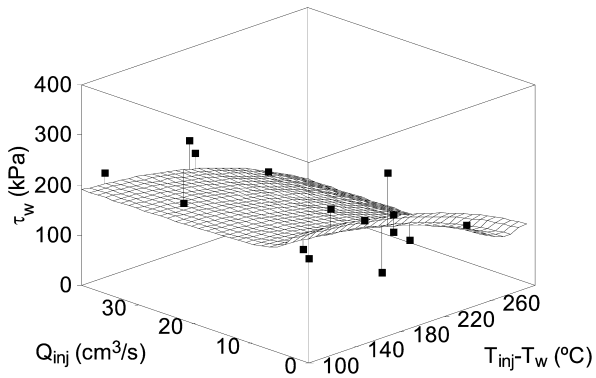

Fig. 5. Variations of the bulk temperature, T_b, and the wall shear stress, τ_w, with the processing variables for the tensile axi-symmetric moulding.

eventual higher viscous dissipation occurring for the higher setting of the processing variable resulting in higher T_b values. For this moulding geometry the variations of τ_w are more dependent on ($T_{inj} - T_w$) than upon Q_{inj}. τ_w decreases with increment in ($T_{inj} - T_w$). A general trend of τ_w to decrease with increasing Q_{inj} is observed, especially for the lower Q_{inj} values and mainly for the highest temperature difference level. These variations are essentially the reflex of changes on the melt viscosity.

Fig. 6 shows the evolution of the computed bulk temperature and maximum shear stress with the processing variables for the disc moulding. The variations of T_b with the processing variables are identical to those of the tensile moulding. Significant differences between these two mouldings are observed in the case of τ_w. For the disc mouldings, τ_w increases significantly with increasing Q_{inj}, and there is a slight trend of τ_w to decrease with ($T_{inj} - T_w$). These two mouldings are placed at extreme positions concerning the variations of the dimensionless numbers, as above shown in Figs. 2–4. The highest heat losses by conduction and low heat dissipation evidenced by the disc moulding may contribute for the shown positive dependences of τ_w upon ($T_{inj} - T_w$). Moreover, for this moulding geometry the melt viscosity seems to be mainly controlled by the shear rate and the temperature differences imposed at

Table 3
Thermomechanical variables and skin ratio values for the three geometries

Moulding geometry									
Run	Tensile axi-symmetric specimen			Laterally gated disc			Box moulding		
	T_b (°C)	τ_w (kPa)	Sa	T_b (°C)	τ_w (kPa)	Sa	T_b (°C)	τ_w (kPa)	Sa
1	204.8	216.7	0.343	191.8	1.73	0.144	219.7	62.2	0.133
2	186.9	285.1	0.642	163.5	0.13	0.511	250.0	52.9	0.141
3	192.3	214.6	0.494	176.2	0.11	0.400	279.3	31.5	0.269
4	203.4	208.7	0.313	191.8	1.04	0.185	220.0	54.8	0.163
5	181.9	191.1	0.627	166.0	0.18	0.436	249.5	28.6	0.239
6	216.8	126.6	0.356	190.7	0.07	0.361	280.0	56.8	0.072
7	231.6	185.3	0.223	230.1	3.14	0.285	219.7	31.4	0.217
8	217.7	167.5	0.331	198.3	0.10	0.359	250.0	62.1	0.086
9	204.5	199.9	0.438	185.7	0.05	0.471	280.0	48.5	0.082
10	215.6	131.3	0.318	196.2	0.10	0.269	–	–	–
11	269.0	100.1	0.175	278.4	2.93	0.253	–	–	–
12	232.7	127.8	0.379	212.4	0.03	0.438	–	–	–
13	247.3	98.6	0.268	230.5	0.11	0.323	–	–	–
14	267.8	94.3	0.114	278.3	3.43	0.107	–	–	–
15	227.0	90.2	0.333	212.5	0.06	0.363	–	–	–
Max	269.0	285.1	0.642	278.4	3.43	0.511	280.0	62.2	0.269
Min	181.9	90.2	0.114	163.5	0.03	0.107	219.7	28.6	0.072
Δ(Max − Min)	47.9	216.0	463.2	70.3	10211.4	379.9	27.5	117.5	273.6

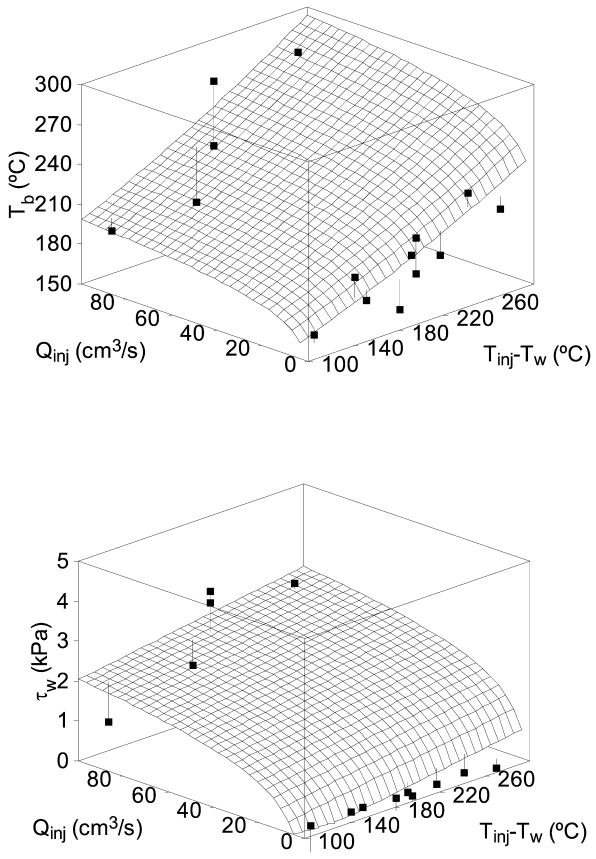

Fig. 6. Variations of the bulk temperature, T_b, and the wall shear stress, τ_w, with the processing variables for the disc moulding.

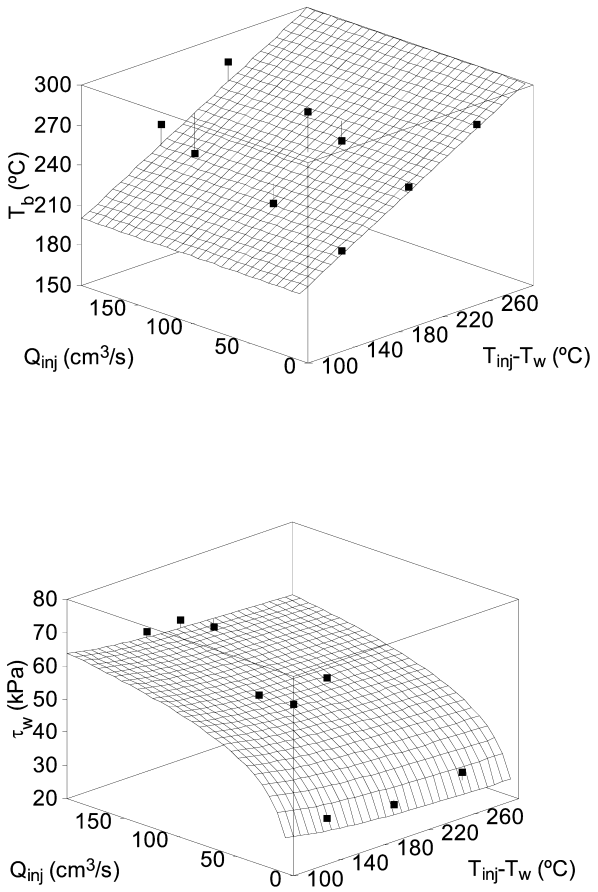

Fig. 7. Variations of the bulk temperature, T_b, and the wall shear stress, τ_w, with the processing variables for the box moulding.

the boundaries (low Br and Na numbers), which is reflected upon the variations of τ_w.

Fig. 7 shows the variations of the computed bulk temperature and maximum shear stress with the processing variables for the box moulding. The evolution of T_b with the processing variables is similar to the other mouldings. T_b shows a high positive dependence upon the imposed temperature differences. The irresponsiveness of T_b upon changes of Q_{inj} may be due to the higher values of Q_{inj} selected for this moulding. In fact, for the other moulding geometries the highest variations of T_b occur for the lower Q_{inj} values, typically lower than 10 cm^3/s. The box moulding shows also a strong dependence of τ_w upon Q_{inj}, as the other plate-like mouldings. However, there is a slight decrement of τ_w with increasing ($T_{inj} - T_w$), as also show by the tensile specimen. This *intermediate* behaviour was already anticipated by the previously variations of the dimensionless numbers with the processing variables.

4.3. Microstructure observations

Figs. 8–10 shows the effect of the operative processing conditions on the microstructure of the mouldings. The tensile specimens show a two-layer microstructure with well defined boundaries: an internal core surrounded by an external skin (Fig. 8). Conversely, the plate-like mouldings present a more inhomogeneous microstructure, where several layers can be distinguished (Figs. 9 and 10). These microstructural differences arise due to the distinct thermo-mechanical environment imposed in the moulding geometries, regardless the similar setting of the operative processing parameters. Furthermore, the configuration of this layered microstructure is also dependent upon the processing conditions for the same moulding geometry. In this work the skin layer was delimited by the boundaries of the shown dark zone.

Figs. 8–10 shows similar trends for the evolution of the skin thickness with the processing conditions for all the moulding geometries. Nevertheless, the magnitudes of the effects are distinct. Fig. 8 depicts the microstructures of the tensile specimens: in the horizontal direction is shown the effect of T_{inj}, while keeping the other parameters constant (T_{inj} increases from left to right); the influence of T_w is presented on the vertical axis (T_w increasing from top to bottom); along the diagonal direction is shown the variations of Q_{inj} (which increase from the left bottom edge to the upper right one). The skin thickness decreases with the increase in the processing parameters. T_{inj} appears as the variable with the strongest influence, followed by Q_{inj} and T_w, as already reported elsewhere [14].

Fig. 9 presents the effect of the processing parameters in the microstructures of the lateral gated discs (only half of the cross-section is shown due to symmetry). For this moulding geometry, Q_{inj} is the processing parameter with the strongest effect on the variations of the skin thickness. T_w plays the less significant role.

For the box mouldings it is not possible to isolate the influence of only one processing parameter due to the selection of the moulding programme. However, the effects can be compared in terms of the imposed thermal and stress levels, as presented in Fig. 10. It seems that changes on the latter are more efficient in varying the skin thickness. Fig. 10 also shows the microstructures of microtomed sections cuts in two directions: in and parallel to the flow direction. In

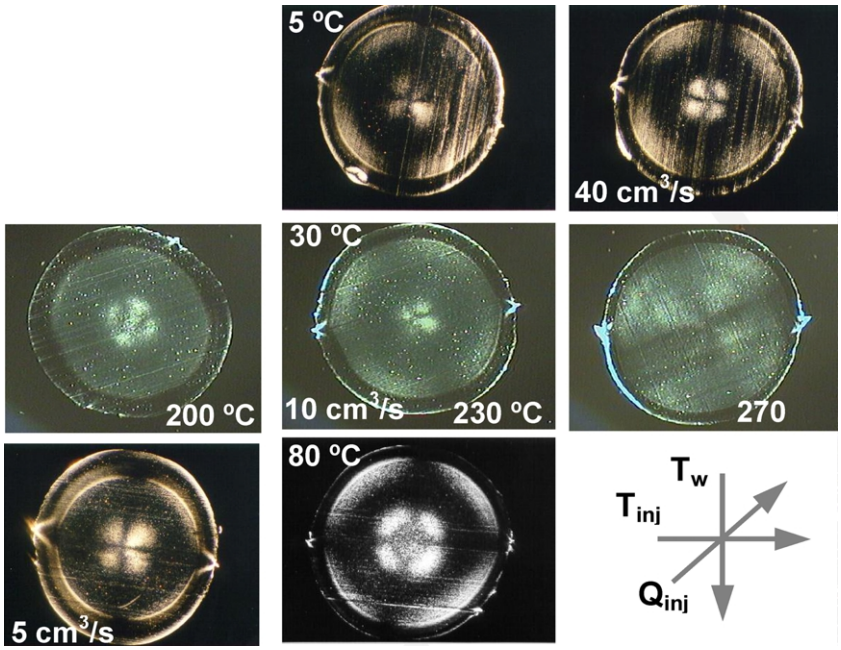

Fig. 8. Effect of the processing variables in the development of the microstructure of the tensile axi-symmetric specimens (the arrows at lower right corner show the direction of increasing of each signed processing variables).

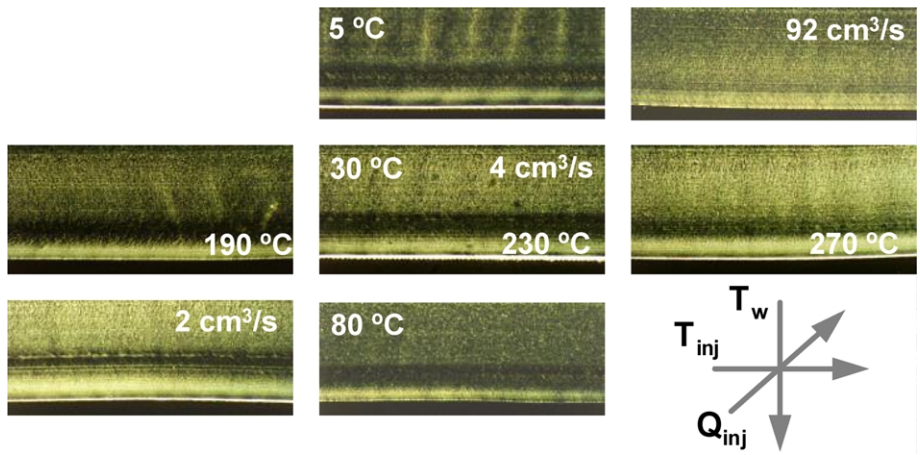

Fig. 9. Effect of the processing variables in the development of the microstructure of the lateral gated discs (the arrows at lower right corner show the direction of increasing of each signed processing variables). Only half of the moulding thickness is shown.

spite of the same trends, the skin boundaries are easier to recognize in the transverse than in the flow direction. Furthermore, the latter gives consistently lower values for the skin thickness. These differences are the reflex of the highly anisotropic character of the skin layer [10,24,25].

In the results presented so far the development of the skin layer was analyzed relative to the variations in the global processing parameters. This approach has been widely followed [1–11], even though that these types of correlations are merely qualitative. More quantitative relationships should be obtained when relating the local thermomechanical environment with the microstructural parameters.

4.4. Skin ratio

Table 3 lists the values of the skin ratios for the three moulding geometries. Fig. 11 presents the variations of Sa with T_b and τ_w for the dumbbell tensile specimens. For this type of flow, Sa is mainly determined by T_b, being inversely proportional to it.

Fig. 12 shows the evolution of Sa with both thermomechanical variables for the disc mouldings. In spite of the highest Ca numbers, the Sa values are lower and the variations less pronounced compared to the tensile specimens (lowest Ca). Again, the predominant effect of T_b on Sa is evidenced, although now also with a slight influence of τ_w. Sa decreases with the increase in both thermomechanical variables.

These types of variations are also presented by the box moulding, as depicted in Fig. 13. The values of Sa for this moulding geometry are the lowest, probably due to the narrow range of variation in the operative processing parameters, also reflected by the lowest variations in the

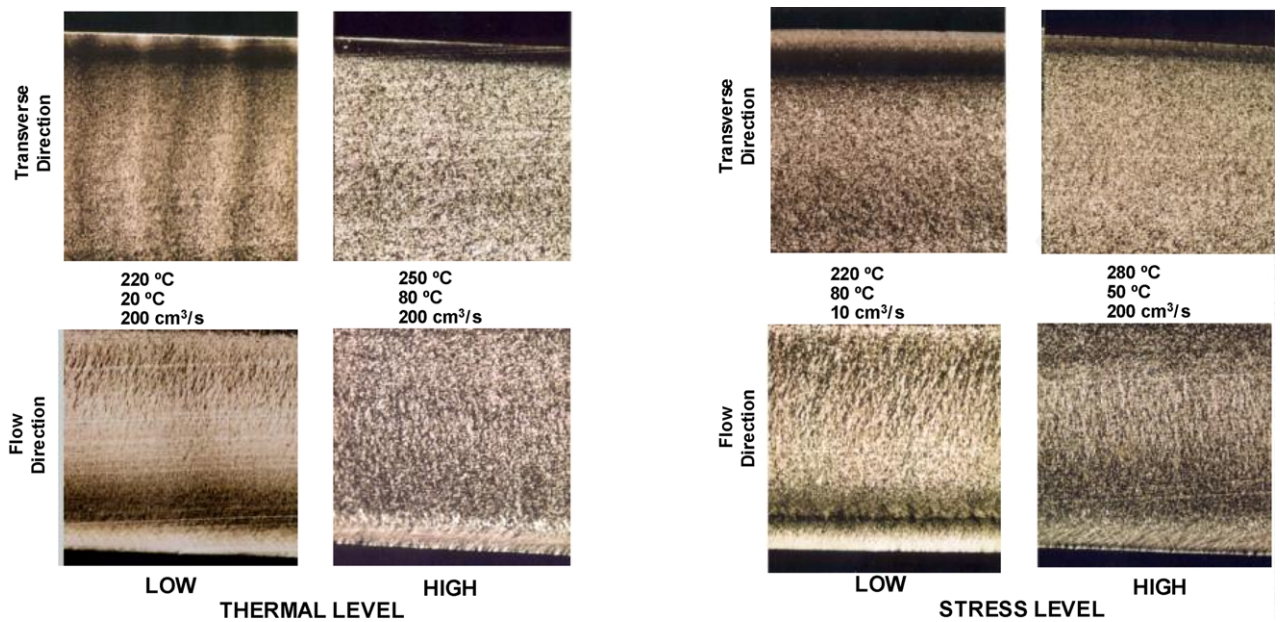

Fig. 10. Effect of the processing variables in the development of the microstructure of the box mouldings.

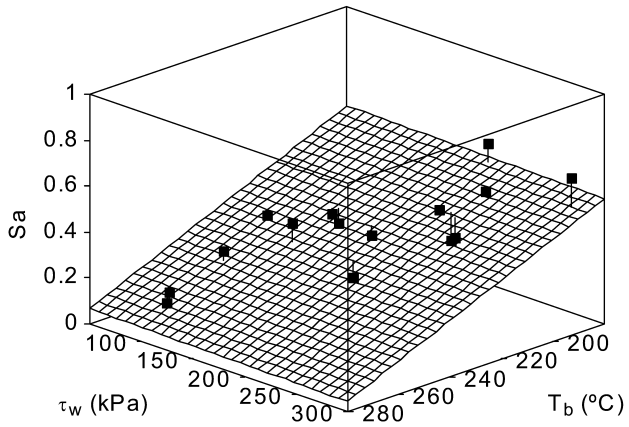

Fig. 11. Variation of the skin ratio, Sa, with the local thermomechanical variables (T_b—bulk temperature; τ_w—wall shear stress) for the tensile axi-symmetric specimens.

thermomechanical variables (Table 3). For the box moulding, Sa is more dependent upon τ_w than on the thermal level.

The evolution of Sa for the three moulding geometries presents the same dependence upon the thermomechanical variables, although with distinct rates of variation and significance of the effects.

5. Discussion

The skin formation is the result of crystallisation under high cooling rates and stress fields. The flow induced molecular orientation cannot completely relax before reaching the crystallisation temperature, T_c, constraining the development of the crystalline structure, and forming highly oriented structures (e.g. shish-kebab structures). The development of the skin layer has been related to two time variables [14]: the time allowed for relaxation of the flow induced molecular orientation until T_c is reached, t_r, and the relaxation time of the material, λ. Generalising, one may assume that:

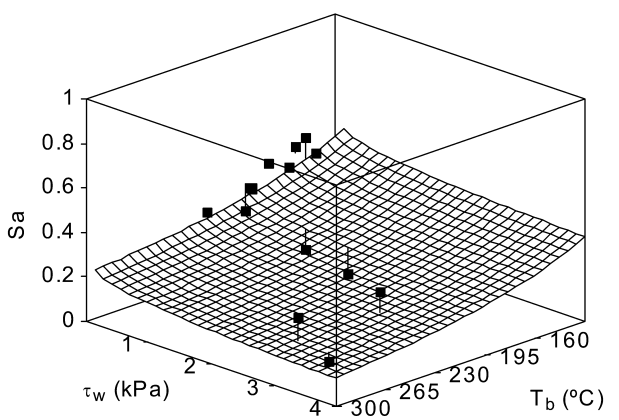

Fig. 12. Variation of the skin ratio, Sa, with the local thermomechanical variables (T_b—bulk temperature; τ_w—wall shear stress) for the lateral gated discs.

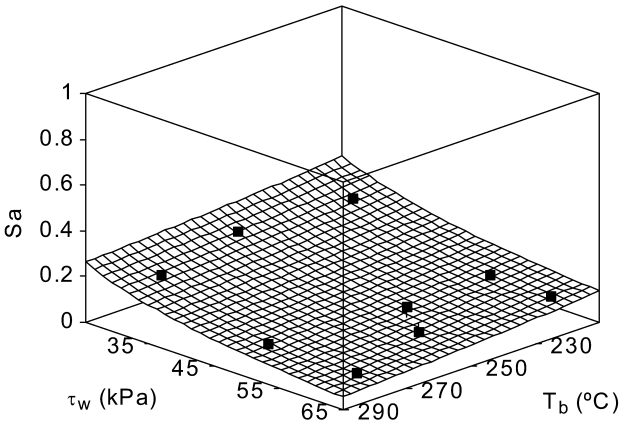

Fig. 13. Variation of the skin ratio, Sa, with the local thermomechanical variables (T_b—bulk temperature; τ_w—wall shear stress) for the box mouldings.

- if $t_r > \lambda$, the flow induced molecular orientation is able to completely relax, leading to the development of spherulitic-like structures
- if $t_r < \lambda$, the flow induced molecular orientation has not enough time to relax before crystallisation, originating the development of a highly oriented skin layer.

Fig. 14 depicts the proposed mechanisms for skin thickening, assuming the thermomechanical conditions that result in skin formation, that is, $t_r < \lambda$. λ increases with the reduction in the shear stress level and in the initial melt temperature, leading to thicker skins. On the other hand, the time to reach T_c decreases with the reduction of the initial melt temperature and the increment of the cooling rate. An increase in T_c (e.g. by the use of nucleating agents) will decrease t_r. This thermomechanical environment results also in thicker skins. It is worthy to note that some of these factors may have opposed effects. An increase in the cooling rate will decrease t_r (thicker skin), but at the same time T_c is decremented (thinner skins). Increasing the injection flow rate will increase the initial melt temperature (thinner skin), but will also increase T_c (thicker skin). The final effect is

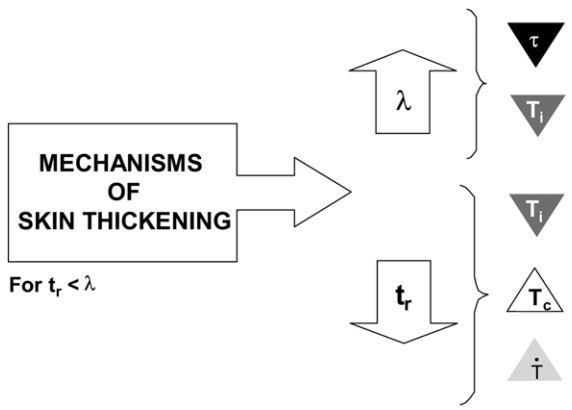

Fig. 14. Mechanisms of skin thickening (assuming $t_r < \lambda$). (τ—shear level, $\dot{T}$—cooling rate, T_i—local melt temperature).

dependent upon the preponderant contribution for the particular applied thermomechanical environment.

The dependences of Sa upon the thermal and mechanical levels above illustrated in Figs. 11–13 can be interpreted in the light of these mechanisms. The strong effect of T_b upon the variation of Sa can be ascribed to the preponderant influence of the thermal level on both t_r and λ : t_r decreases and λ increases with the decrement in the temperature, leading to an increment in the skin thickness. The slight decrease of Sa with τ_w can be attributed to the reduction of λ, which is counter-balanced with the increment in T_c.

In injection moulding the cooling stage is essentially a heat transfer phase, where the heat input by the hot molten polymer must be removed by the implemented mould cooling system (cooling channels). The time to reach the crystallization temperature, t_r, can be estimated by the exact solution of the conduction Fourier equation [30]:

$$\theta = \frac{T_w - T_c}{T_w - T_i} = 2\sum_{n=0}^{\infty} \frac{(-1)^n}{(n+1/2)\pi} \exp\left[-(n+1/2)^2\pi^2 \frac{\alpha t_r}{h^2}\right] \cos\left[(n+1/2)\frac{\pi y}{h}\right] \quad (1)$$

where y is the thickness coordinate, h is the moulding half-thickness, α is the thermal diffusivity and T_i the initial material temperature. After the filling phase and for a given y position (that is, initial local temperature) the time to reach T_c shows a logarithmic trend upon the dimensionless temperature difference, θ. On the other hand, the material relaxation time, λ, depends exponentially upon the inverse of the temperature, T. In a simple analysis (assuming a single relaxation time), the temperature dependence of λ is of the form:

$$\lambda(T) = A\, e^{\frac{B}{T}} \quad (2)$$

where A and B are material constants. λ is also influenced by shearing and pressure level applied to the melt, but the simultaneous consideration of all these effects is not trivial (it can be assumed that they may affect the constant A of Eq. (2)). Nevertheless, λ is inversely proportional to the shear and pressure levels.

In Fig. 15 is represented the expected variations of t_r and λ through the moulding thickness due to an imposed thermal gradient (an initial arbitrary through-the-thickness temperature profile is assumed). The transition point ($t_r = \lambda$) defines the boundary between the formation (right side) and the non-development (left side) of a skin layer. This model will be used to interpret the effect of processing in the development of the skin layer as above experimentally detailed, but by isolating the influence of each processing variable upon the position of this transition point ($t_r = \lambda$).

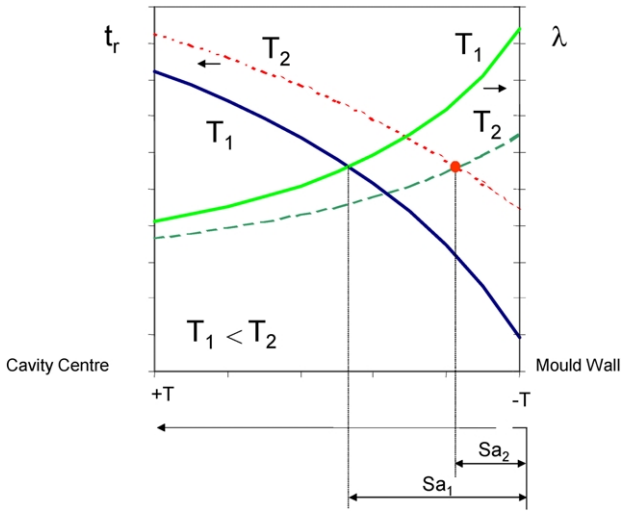

Fig. 15. Variations of the time to reach the crystallization temperature, t_r, and the material relaxation time, λ, through the moulding thickness due to an increasing in the melt temperature, T_b.

5.1. Melt bulk temperature

The bulk temperature of the material is mainly controlled by melt and mould temperatures and, in a less degree, by the flow rate (Figs. 5–7). In general, the highest is the setting of these operative variables the highest T_b will be. Increasing T_b increments t_r and reduces λ. Both these changes contribute for the strong reduction of the skin thickness with T_b, as illustrated in Fig. 15. The transition point ($t_r = \lambda$) is significantly moved to the right side (skin thinning) by the increment of T_b.

The skin ratio presents therefore a strong dependence upon T_b (as evidenced by all the moulding geometries, Figs. 11 and 13).

5.2. Mould temperature

The skin thickness is also determined by the cooling rate, which can be effectively controlled by changing T_w. The effect of this reduction upon the variations of t_r and λ is shown in Fig. 16.

A decrease in T_w (or increment in the cooling rate) will reduce t_r (Fig. 16a), with negligible influence on λ. This will move the transition point into the cavity mid-plane (left side), increasing the skin thickness. On the other hand, this reduction in T_w will decrease T_c, increasing t_r and resulting in a thinner skin (Fig. 16b). The influence of the mould temperature upon the development of the skin thickness has therefore opposed effects, resulting in a lower contribution of this variable for the development of the skin thickness.

5.3. Injection flow rate

The injection flow rate controls the shear rate level, $\dot{\gamma}$, imposed to the material during the filling stage. Higher Q_{inj} values lead to an increment (or less reduction) of the material bulk temperature at the end of the filling due to a

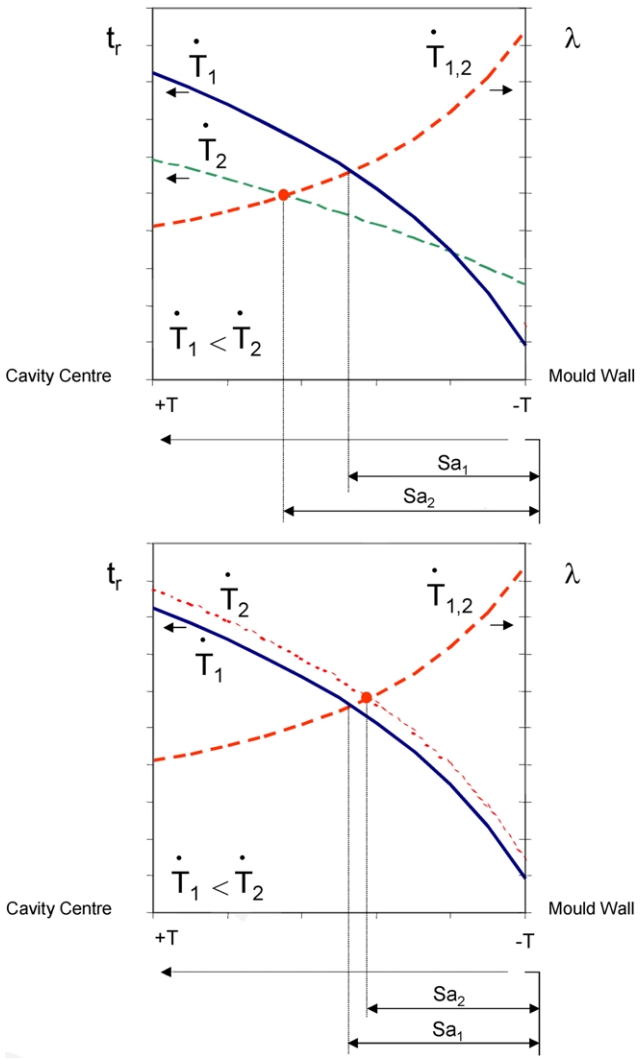

Fig. 16. Variations of the time to reach the crystallization temperature, t_r, and the material relaxation time, λ, through the moulding thickness due to an increase in the cooling rate originated by: (a) a decrease of the mould temperature, T_w; (b) a decrease in T_c.

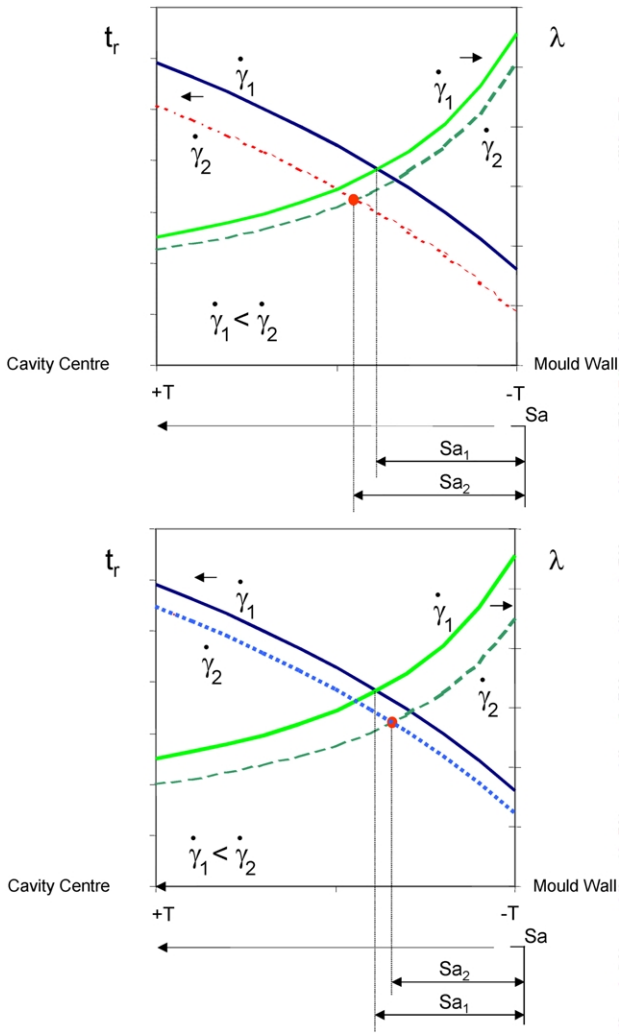

Fig. 17. Variations of the time to reach the crystallization temperature, t_r, and the material relaxation time, λ, through the moulding thickness due to an increasing in strain rate originated by: (a) a major effect on t_r; (b) a major effect upon λ.

lower heat conduction and probable higher heat dissipation (that is, lower Ca and higher Br numbers). But, in order to consider independently both these effects (the increase in T_b and the isolated change in the shear rate) they will be treated separately. The first case has been already dealt with above, and only the isolated effect of the shear rate will be analysed. The cooling rate will be thus assumed constant (that is, T_b and T_w both are constant). An increase in $\dot{\gamma}$ will have two distinct effects: (i) T_c increases, reducing t_r; and (ii) λ is reduced. That is, both t_r and λ are decreased. Depending on the magnitude of these opposed effects, the development of the skin layer will be distinct (Fig. 17).

If the highest contribution is the reduction in t_r, increasing $\dot{\gamma}$ will result in a thicker skin layer (Fig. 17a). On the other hand, if the main effect is the reduction in λ, the skin will be thinner (Fig. 17b). However, the concomitant increase in T_b due to higher $\dot{\gamma}$ causes the reduction in λ and the increment in t_r, leading to skin thinning. The final balance seems to be the reduction of Sa with the increase of $\dot{\gamma}$.

5.4. Moulding geometry

The variations of Sa for the three moulding geometries present the same dependence upon the thermomechanical variables, although with distinct rates and significance of the effects. This may be attributed, at some extent, to the different relative importance of the principal physical phenomena occurring and their distinct degree of interaction, as already revealed by the variations of the dimensionless numbers.

The tensile specimens show an exclusive dependence of Sa upon T_b. The quasi-adiabatic regime and high viscous dissipation may contribute for this. Furthermore, τ_w is controlled by the thermal level, decreasing with it (Fig. 5). This thermomechanical environment points for a strong dependence of Sa upon T_b : the concomitant decrease of the thermal and shear level favours the skin thickening (see Fig. 14).

The disc mouldings evidence the highest heat losses by conduction and the lower viscous dissipation. The τ_w values are the lowest and mainly controlled by Q_{inj}, increasing with it. However, the evolution of T_b with the processing variables is similar to those of the tensile specimens (compare Figs. 5 and 6, respectively). Furthermore, the disc mouldings show a reduced variation of Sa when compared to the tensile specimens (Table 3). Two opposed effects seems to intervene. On the one hand, the decrease of the thermal level (that is T_b) leads to thicker skin layers (Fig. 14). On the other hand, the increase in the shearing level (that is Q_{inj}) reduces the thickness of the skin. These opposed effects result in a smaller contribution of the thermal level as compared with the tensile specimen geometry, and a slight higher influence of τ_w in the development of the skin layer.

The temperature profile for the box moulding is developed under a quasi-adiabatic regime and relatively low viscous dissipation. τ_w is basically determined by Q_{inj} in the same way as for the disc mouldings but now having higher values. Again, two distinct contributions seem to play opposed roles. However, the box moulding presents a higher contribution of the shear level than the thermal one to the development of the skin thickness. This may be attributed to the narrow range of variation of the thermal level.

The main differences relating the development of the skin layer on all the moulding geometries appears to be due to the effect of τ_w, which has distinct dependences upon variation of the operative processing variables. This points out for the decisive effect of the shear level upon the development of the skin (shear induced crystallization) and the high interaction between the thermal and mechanical fields.

6. Conclusions

This work analyses the development of the skin layer in injection moulding for different moulding geometries and processing conditions. The thermomechanical environment was characterized by calculation of dimensionless numbers (Cameron, Brinkman and Nahme) and thermomechanical variables computed from mould filling simulations. The skin ratio was related to the local bulk temperature and maximum shear stress at the end of the filling phase. This type of relationships between the processing conditions and the microstructure must be established locally, relating the local thermomechanical environment to the microstructure (and morphology) development. The mechanisms of formation of the skin layer were proposed, which are related to the time to reach the crystallization temperature and the material relaxation time. The main conclusions are:

- The skin thickness increases with the decrease in both thermal and shear levels (for all moulding geometries).
- Variations in the melt temperature have a strong effect on the development of the skin layer. The increase in the melt temperature results in the increment in the time to reach the crystallization temperature and in the reduction of the material relaxation time, both effects contributing for the skin thinning mechanisms.
- The effect of the mould temperature has two opposed effects. Decreasing the mould temperature increases the cooling rate, which reduces the time to reach the crystallization temperature (thicker skin), but it also decreases the crystallization temperature increasing the time to reach the crystallization temperature (thinner skin). Therefore, this operative variable has, in general, a low contribution for the development of the skin layer.
- The increase of the injection flow rate increases the temperature and shearing level of the melt. The latter phenomena have two different effects: it increases the crystallization temperature hence reducing the time to reach the crystallization temperature (thinner skin); and it decreases the material relaxation time (thinner skins). The development of the skin layer is dependent upon the magnitude of the major effect. However, the concomitant increase of the melt temperature imposed by the higher flow rates leads to skin thinning. The final balance seems to be the reduction of skin thickness with increasing injection flow rate.
- The moulding geometry has a great influence on the imposed shear stress level. The effect of the operative processing conditions on the shear stress level is dependent upon the moulding geometry. This controls the development of the skin layer.

The proposed phenomenological model is able of interpreting the effect of the processing conditions (operative variables and mould geometry) on the development of the skin layer. This is governed by distinct factors that can operate with opposed contributions, evidencing a strong interaction between the thermal and mechanical levels imposed during processing.

Acknowledgements

This work was financially supported by FCT-foundation for Science and Technology, through the FOCTI and FEDER programmes.

References

[1] Kantz MR, Newman HD, Stigale FH. J Appl Polym Sci 1972;16:1249.
[2] Schultz JM. Polym Engng Sci 1984;24:770.
[3] Trotignon J-P, Verdu. J Appl Polym Sci 1987;34:1–18.
[4] Fujiyama M, Wakino T. Intern Polym Proc 1992;VII(1):97–105.
[5] Phillips R, Herbert G, News J, Wolkowicz J. J Polym Engng Sci 1994; 34(23):1731–43.
[6] Zipper P, et al. Intern Polym Proc 1995;X(4):341–50.

[7] Zipper P, Abuja PM, Jánosi A, Wrentschur E, Geymayer W, Ingolic E, Friesenbichler W. Polym Engng Sci 1996;36(4):467–82.
[8] Kalay G, Bevis MJ. J Polym Sci: part B: Polym Phys 1997;35: 265–91.
[9] Liu GW, Zhu PW, Edward G. Macromol Symp 2002;185:327–40.
[10] Fujiyama M. In: Karger-Koscis J, editor. Polypropylene structure, blends and composites: structure and morphology, vol. 1. London: Chapman and Hall; 1995. p. 167–204.
[11] Fujiyama M, Waklino T. J Appl Polym Sci 1991;42(10):2739–47.
[12] Gahleitner M, Wolfschwenger J, Bachner C, Bernreitner K, Neißl W. J Appl Polym Sci 1996;61(4):649–57.
[13] Viana JC. PhD thesis, University of Minho; 2000.
[14] Viana JC, Cunha AM, Billon N. Polymer 2002;43:4185–96.
[15] Cunha AM, Godinho JS, Viana JC. Structure development during polymer processing. In: Cunha AM, Fakirov S, editors. Nato Science Series, Series E: Applied Science, vol. 370. Dordrecht: Kluver Academic; 2000. p. 255–77.
[16] Viana JC, Cunha AM, Billon N. Polym Engng Sci 1999;39(8): 1463–72.
[17] Cunha AM, Pouzada AS. In: Williams JG, Pavan A, editors. Impact and dynamic fracture of polymers and composites, ESIS19. London: Mech. Eng. Public; 1995. p. 315–25.
[18] Viana JC, Cunha AM, Billon N. J Mat Sci 2001;36(18):4411–8.
[19] Richardson SM. In: Tucker CL III, editor. Fundamentals of computer modeling for polymer processing. New York: Hanser publishers; 1989. p. 113–40.
[20] Bay RS, Tucker III CL, Davis RB. Tech Papers SPE ANTEC'89 1989;539–42.
[21] CMOLD® Reference Manual, AC Technology; 1996.
[22] Viana JC, Cunha AM, Billon N. Intern Polym 1997;43:159–66.
[23] Viana JC, Cunha AM, Billon N. Tech Paper SPE ANTEC'2000 2000; paper 111.
[24] Wening W, Herzog F. J Appl Polym Sci 1993;50:2163–71.
[25] Fujiyama M, Wakino T, Kawasaki Y. J Appl Polym Sci 1988;35: 29–49.
[26] Saiu M, Brucato V, Piccarolo S, Titomanlio G. Intern Polym Proc 1992;VII(3):267–73.
[27] Brito AM, Cunha AM, Pouzada AS, Crawford RJ. Intern Polym Proc 1991;VI(4):370–7.
[28] Demiray M, Isayev AI. Tech Papers SPE, ANTEC'96 1996;II: 1576–80.
[29] Jerschow P, Janeschitz-Kriegl H. Intern Polym Proc 1997;XII(1): 72–7.
[30] Agassant JF, Avenas P, Sergent J-Ph. Polymer processing and modeling. Munich: Carl Hanser; 1991.